Observations of Stratospheric Gravity Waves Over Europe on 12 January 2016: The Role of the Polar Night Jet

Katrina Bossert[1,2], Sharon L. Vadas[3], Lars Hoffmann[4], Erich Becker[3], V. Lynn Harvey[5], Martina Bramberger[3]

[1]School of Earth and Space Exploration, Arizona State University, Tempe, AZ, 85287

[2]School of Mathematical and Statistical Sciences, Arizona State University, Tempe, AZ, 85287

[3]NorthWest Research Associates, Inc., 3380 Mitchell Lane, Boulder, CO 80301, USA

[4]Julich Supercomputing Centre, Forschungszentrum Jülich, Jülich, Germany

[5]Laboratory for Atmospheric and Space Physics, University of Colorado Boulder, Boulder, CO, USA

Abstract:

Observations during 12 January 2016 revealed a series of events of significant gravity wave (GW) activity over Europe. Analysis of derived temperatures from the Atmospheric InfraRed Sounder (AIRS) provides insight into the sources of these GWs, and include a new observation of stratosphere polar night jet (PNJ) generated GWs. Mountain waves were present during this time as well over the French Alps and the Carpathian Mountains, and had maximum temperature perturbations, *T'*, as large as 27K over the French Alps. Further investigation of the mountain waves demonstrated their presence in the stratosphere was not only determined by stratospheric conditions, but also by strong winds in the troposphere and at the surface. GWs generated in the stratosphere by the PNJ had maximum *T'* of 7K. These observations demonstrate multiple sources of GWs during a dynamically active period, and implicate the role of the PNJ in both the vertical propagation of GWs generated in the troposphere and the generation of GWs from the PNJ itself.

Key points

- AIRS observations demonstrate the presence of gravity waves generated by the polar night jet
- Downward propagating gravity waves were observed at altitudes below the polar night jet
- The polar night jet plays an important role in the growth of mountain waves in the stratosphere

1. Introduction:

Gravity waves (GWs) play an important role in coupling across regions of the atmosphere through the vertical transport of momentum. It is well known that the deposition of momentum from breaking GWs in the mesosphere and lower thermosphere drives a residual circulation between the summer and winter hemispheres and thereby induces the cold summer mesopause and the warm winter stratopause, as well as a reversal of the summer mesospheric jet [*Holton, 1982, 1983; Garcia and Solomon, 1985; Fritts and Alexander, 2003*]. While the influences of GWs on global circulation are well known from modelling efforts, there are still uncertainties in the parameterization of GWs in global scale models regarding GW sources within the atmosphere, and subsequent deposition of GW momentum into the middle atmosphere [*Alexander et al.*, 2010]. For example, the structure of the winter hemispheric mesospheric jet likely has dependence on secondary GWs generated in the stratopause region [*Becker and Vadas*, 2018], but secondary GWs are not included in conventional GW parameterizations.

Satellite measurements have led to global scale studies of stratospheric GWs, improving knowledge about GW sources and associated hotspot regions. Stratospheric GW measurements include global observations from the Atmospheric InfraRed Sounder (AIRS) [*Gong et al*., 2012; *Hoffmann et al*., 2013; *Eckermann et al*., 2019; *Schmidt et al*., 2016], the Cloud Imaging and Particle Size (CIPS) instrument [*Randall et al*., 2017], the High Resolution Dynamics Limb Sounder (HIRDLS) [*Ern et al.*, 2018], the GPS Meteorology experiment [*Tsuda et al.*, 2000], Sounding of the Atmosphere using Broadband Emission Radiometry (SABER) [*Liu et al*., 2019], and the Microwave Limb Sounder (MLS) [*Jiang et al*., 2003; *Wu et al*., 2008]. AIRS has provided the opportunity to study GWs through radiance perturbations [*Alexander and Barnet,*

2007]. AIRS also allows for temperature retrievals both spatially and vertically through a high-resolution retrieval scheme detailed in Hoffmann and Alexander (2009). This temperature retrieval has previously been validated and used for the study of GWs [*Ern et al.*, 2017; *Wright et al.*, 2017; *Meyer et al.*, 2014]. The AIRS high-resolution retrievals are limited to GWs with long vertical wavelengths with λ_z>~15km. Retrieved temperatures have a vertical resolution which changes with height, varying from a 7km resolution near 20km in altitude to a 12-14km resolution near 55km in altitude. AIRS observations have led to global studies of stratospheric GW hotspot regions associated with tropospheric GW sources including convectively and orographically generated GWs [*Hoffmann et al., 2016*; *Hoffmann et al., 2014; Gong et al., 2012; Jiang et al., 2012; Jiang et al., 2005*].

Favorable conditions within the stratosphere can allow for GW propagation to higher altitudes. The polar night jet (PNJ) plays an important role in filtering stratospheric GWs in winter time. Many observational and modeling studies have shown that under conditions of significant stratospheric winds such as those winds associated with a strong PNJ, mountain waves (MWs) can propagate into the stratosphere and mesosphere [*Fritts et al, 2016; Eckermann et al., 2016; Bossert et al., 2015; Kruse et al., 2016; Vadas and Becker, 2018; Dörnbrack et al., 2002*]. Strong stratospheric winds associated with the PNJ allow for growth to large vertical wavelengths and amplitudes [*Alexander and Teitelbaum*, 2007; *Wright et al.*, 2017; *Bramberger et al., 2017; Gisinger et al., 2017; Ehard et al., 2017a; Heale et al.*, 2017; *Dörnbrack et al.*, 1999]. In addition, GWs having intrinsic horizontal phase propagation against the background wind are focused into the wind maximum due to horizontal refraction [*Senf and Achatz*, 2011; *Preusse et al*., 2009; *Ehard et al*., 2017b; *Jiang et al*., 2019]. Other observations have

demonstrated a positive correlation between GW activity and wind speed in the stratosphere [*Chu et al., 2018; Llamado et al*., 2019].

In addition to controlling the propagation and dissipation of GWs, both the PNJ and tropospheric jets can be a source of GWs due to spontaneous emission [*Plougonven and Snyder*, 2007; *Sato and Yoshiki*, 2008*; Plougonven and Zhang,* 2014; *Uccellini and Koch*, 1987]. Observations have linked measured GWs to the tropospheric jets as a source region [*Sato and Yoshiki*, 2008; *Buss et al., 2004; Wu and Zhang, 2004*]. Furthermore, modeling studies show GW generation from the tropospheric jets [*O' Sullivan and Dunkerton*, 1995; *Zhang et al*., 2004; *Wang et al*., 2008; *Sato,* 2000; *Sato et al.*, 1999]. Additionally, GWs can be generated from disruptions of the PNJ due to sudden stratospheric warmings [*Dörnbrack et al*., 2018; *Yamashita et al*., 2010; 2013].

This paper examines an active GW day over Europe on 12 January 2016. Data used include derived temperature perturbations from AIRS, and the Modern-Era Retrospective analysis for Research and Applications, Version 2 (MERRA-2) [*Bosilovich et al*., 2015; *Molod et al*., 2015]. During this case study, the PNJ and the tropospheric jet overlapped the region of observation, resulting in a strong west to east flow over the Alps. The sources of GWs are investigated, and include MWs and stratospheric GWs generated by the PNJ. This study explores the concurrent nature of these different GW sources.

2. AIRS Observations of GW Activity over Europe on 12 January 2016

On 12 January 2016, the AIRS instrument observed significant temperature perturbations associated with GWs over central Europe. The temperature perturbations, obtained from the AIRS high-resolution temperature retrieval of Hoffmann and Alexander (2009), were visible over a range of altitudes from ~20km-60km, and over a range of times between 0.3UT and

13.1UT. Background average temperatures were subtracted across each latitude and altitude to obtain *T'*. Examples of GW derived *T'* observed in AIRS for the two events in the earlier part of the day are shown in Figure 1. AIRS 4.3μm daily average brightness temperature variances following Hoffmann et al. (2013) are plotted over the strength of the polar night jet at 30km for this day and shown in Figure 2. The gray lines denote the polar vortex edge determined using the method described in Harvey et al. (2002). The locations of three separate events are labeled on this plot. Event 1 and 2 are discussed in this paper. Event 3 is not included in this discussion as the GWs may come from a different source than those GWs observed in events 1 and 2 at earlier times in the day. However, event 3 is labeled here as it contributes a significant variance in AIRS brightness temperatures over the daily average.

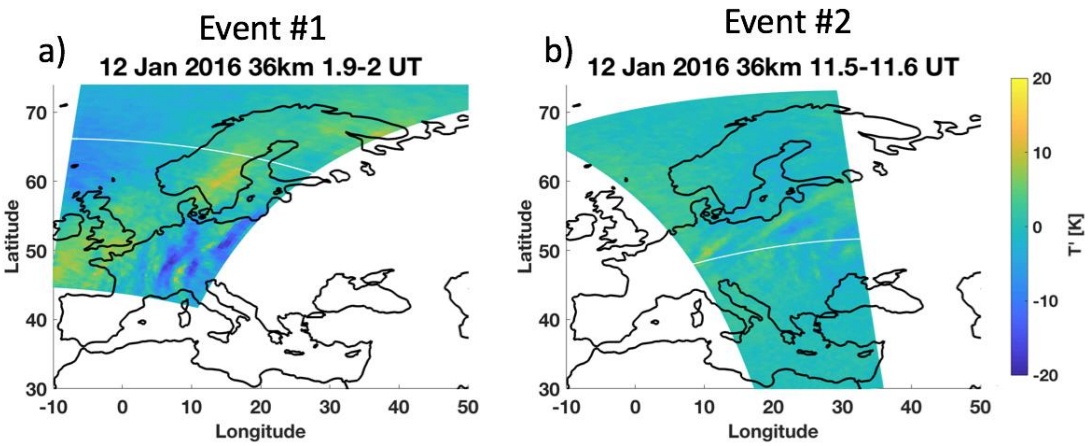

Figure 1: Two separate GW events observed in AIRS on 12 January 2016. Derived *T'* are plotted at 36km. Granule swaths were taken at a) 1.9 and 2 UT, b) 11.5 and 11.6 UT. White lines in each plot denote the boundary of the granule from AIRS.

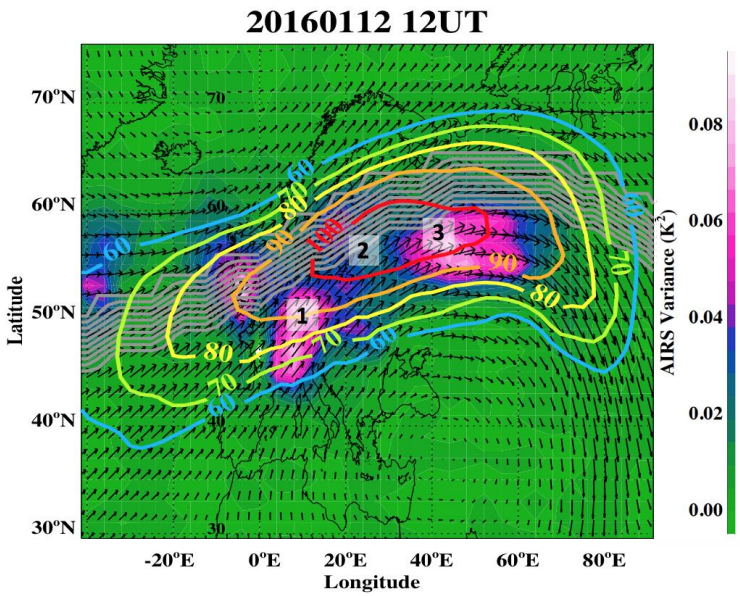

Figure 2: The strength of the PNJ at 30km plotted over the AIRS 4.3μm brightness temperature variance. Isotachs represent magnitude wind speeds in ms^{-1}, and the cluster of gray lines denote the edge of the polar vortex derived from MERRA-2 at 12UT. Three regions of significant GW variance are numbered 1-3. Events from regions 1 and 2 are shown in Figure 1.

2.1 Event 1: Mountain Wave Generation over the Alps

Near 2UT on 12 January 2016, strong GWs were observed in AIRS with *T'* maximum amplitudes reaching ~27K near 50km in altitude. Plots of spatial *T'* at 42km in altitude and vertical *T'* profiles along a longitude-altitude section are shown in Figures 3a and 3b. These GWs had horizontal wavelengths of ~230km, and are visible up to 60km at this time. Later observations at 13.1 UT (Figures 3c and 3d) show that the measured *T'* associated with these GWs has significantly decreased, with *T'* <5K. Figure 3c shows that they are visible at 36km with much weaker amplitudes, but are not visible above this region.

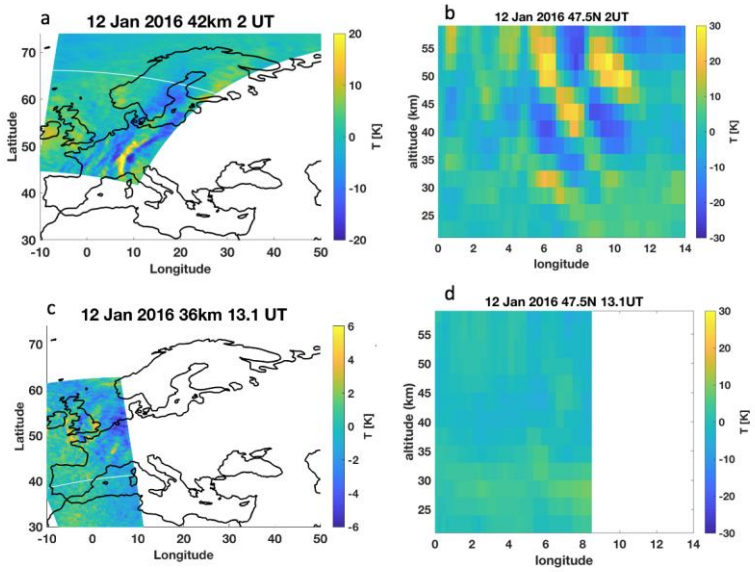

142

143 Figure 3: AIRS T' derived for 'a' 42km in altitude at 2UT, 'b' a vertical section along 47.5N at
144 2UT, 'c' at 36km altitude at 13.1UT where there is still some evidence of a MW, and 'd' a
145 vertical section along 47.5N similar to 'b' and plotted on the same scale, demonstrating the
146 difference in T' amplitudes between the two times.

147 The large amplitude GWs shown in Figures 3a-b arise over the Alps during a time of
148 overlap with the tropospheric jet. MERRA-2 wind vectors at 11km plotted over the topography
149 [*Amante et al.*, 2009] at 0UT on 12 January are shown in Figure 4a, and the wind magnitudes are
150 plotted in Figure 4b. The wind vectors show the tropospheric jets are overlapped with the Alps,
151 with wind vectors nearly perpendicular to the western Alpine ridge near 8^{o}E, 47.5^{o}N. The
152 orientation of the large amplitude GWs observed by AIRS in Fig. 3b indicates a westward
153 propagation direction assuming upward propagating MWs, which is against the eastward winds
154 shown in Figure 4a. The propagation against the direction of the wind in the upper troposphere in
155 combination with the orientation of the GW over the Alpine ridge indicates that the observed
156 wave is a mountain wave (MW). Additionally, the winds shown in Figure 5 indicate for a MW
157 (c=0m/s), the vertical wavelength near z=40km would be ~20km, which is in line with AIRS

observations given in Figure 3b. This MW event and subsequent propagation into the mesosphere and lower thermosphere was the subject of a modeling study by Heale et al. (2020), which predicted MW breaking occurring from 60-80km.

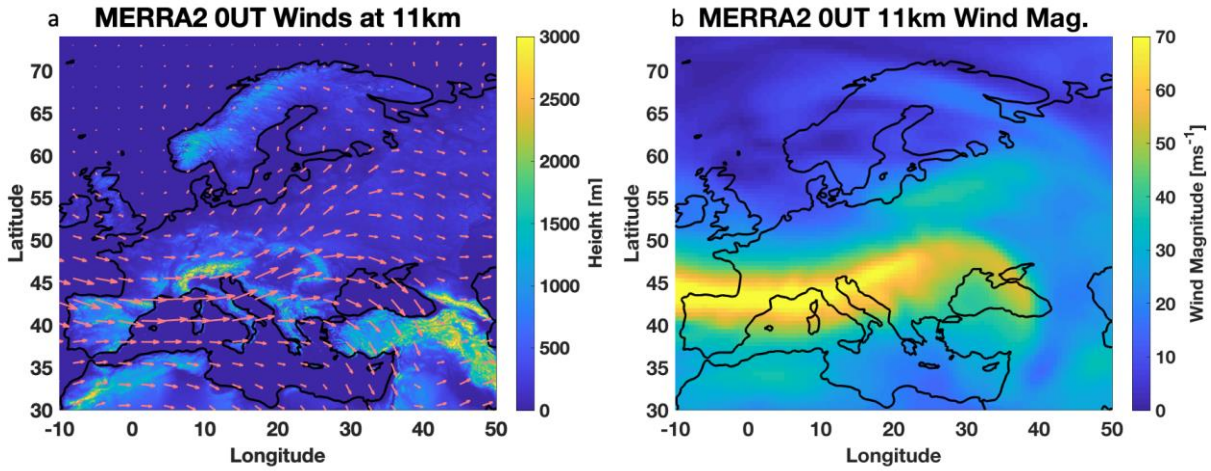

Figure 4: Plot 'a' shows MERRA-2 wind vectors in red at 11km and 0UT plotted over a topographic map of Europe, and Plot 'b' shows MERRA-2 wind magnitudes at 11km. The wind vectors show the tropospheric jets are overlapped with the Alps during this time.

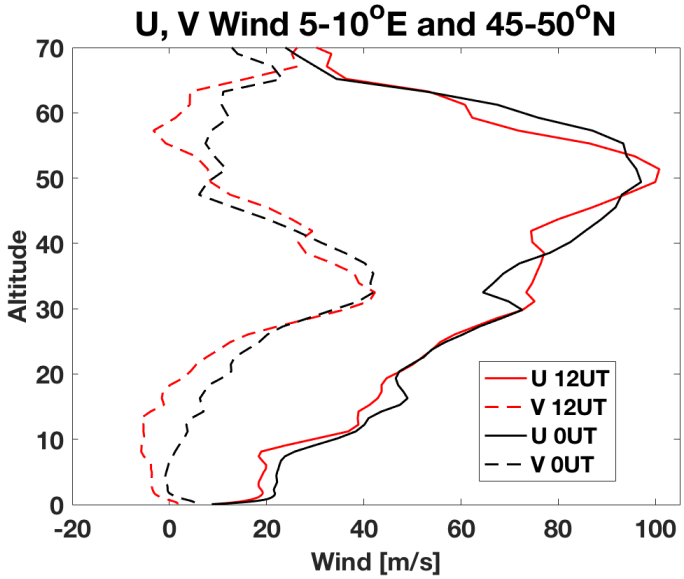

Figure 5: MERRA-2 zonal and meridional winds averaged from 5-10^{o} E, 45-50^{o} N at 0UT and 12UT near the observation times and regions of the strong MWs and weak MWs respectively.

A significant change in MW *T'* amplitudes was observed between 2 UT and 13.1 UT, which may be due to changes in the background winds or forcing conditions. MERRA-2 zonal winds at 0UT and 12UT over 5-10^{o} E and 45-50^{o} N are plotted in Figure 5. While MERRA-2 shows wind profiles which are similar in the stratosphere between the two times, another possibility contributing to the difference in observed MWs is a change in the wind forcing of MWs near the surface. Figure 6 gives a comparison of MERRA-2 winds between 11-12 January near the surface on the western side of the French Alps at 6.25^{o}E and 45^{o}N. The highest peaks in the Alps are above 4km, with the ridge being above 3km. The location chosen in Figure 6 shows winds for altitudes above 2km, which is about halfway in altitude of the highest peaks on the French Alps. Figure 6 demonstrates a strengthening in the zonal winds in the lower troposphere starting near 12UT on 11 January, maximizing near 21UT, and followed by winds decreasing to less than half of the previous magnitude by 6UT on 12 January. During this time duration on 11 January, meridional winds are close to zero near the surface, thus the forcing is largely dominated by zonal winds. In order to determine the duration it took for MWs to propagate to ~50km in altitude of a MW, the mid-frequency approximation for GWs was used (e.g. Fritts and Alexander, 2003) to determine the vertical group velocity, $c_{gz} \approx \frac{k_H}{N} U^2$, where k_H is the horizontal wavenumber, N is the buoyancy frequency, and U is the zonal wind, and the MW is assumed to be propagating approximately zonally. The vertical group velocity was calculated using MERRA-2 winds and temperatures, then integrated over each altitude bin to obtain an approximate time of propagation from the surface to ~50km at launch times of 15UT and 21UT on 11 January, and 0UT on 12 January. The propagation times were found to be 4.5 hrs, 5.7 hrs, and 5.3 hrs respectively, indicating that the observed MW at 2UT on 12 January was most likely forced near the time of the surface wind maximum on 11 January. Given that the observed MWs

ranging from the entire AIRS vertical observation altitudes of z=20-60km, MWs were likely forced over several hours during this time period of maximized surface winds on 11 January. The weakening surface winds on 12 January are likely the reason for the lack of MWs observed at 13.1 UT.

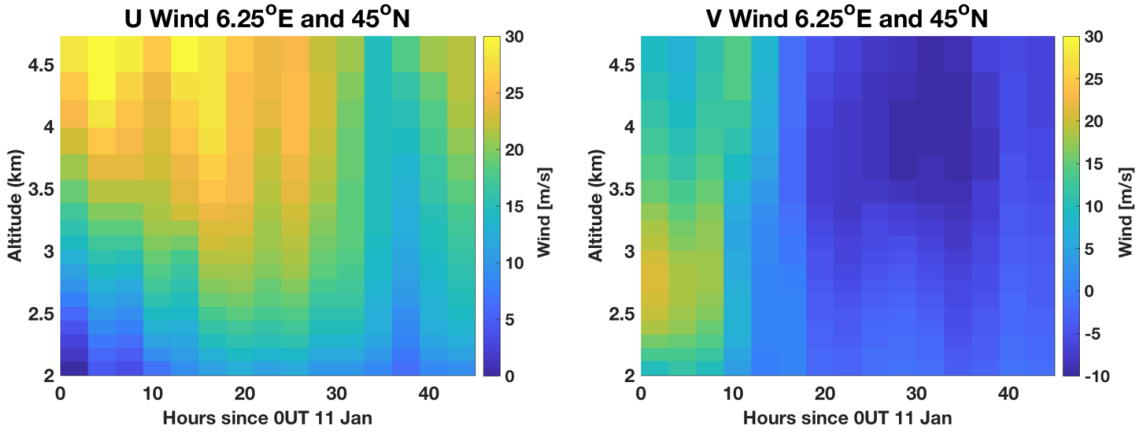

Figure 6: Altitude-time section of MERRA-2 left) zonal winds and right) meridional winds plotted every 3 hours from 00 UT 11 January through 12 January from the surface to 4.7km.

Trailing Mountain Waves and Gravity Waves Towards the East

Shortly before the observation of the MWs at 2UT, AIRS observed GWs further towards the East at 0.3UT. The GW T' measurements from AIRS are shown with the MW measurements at altitudes of 30km and 48km with wind vectors from MERRA-2 in Figure 7. For trailing GWs to be present, one would expect these waves to be downwind of the wind vector [*Jiang et al.*, 2019], and this is indeed the case for these observations.

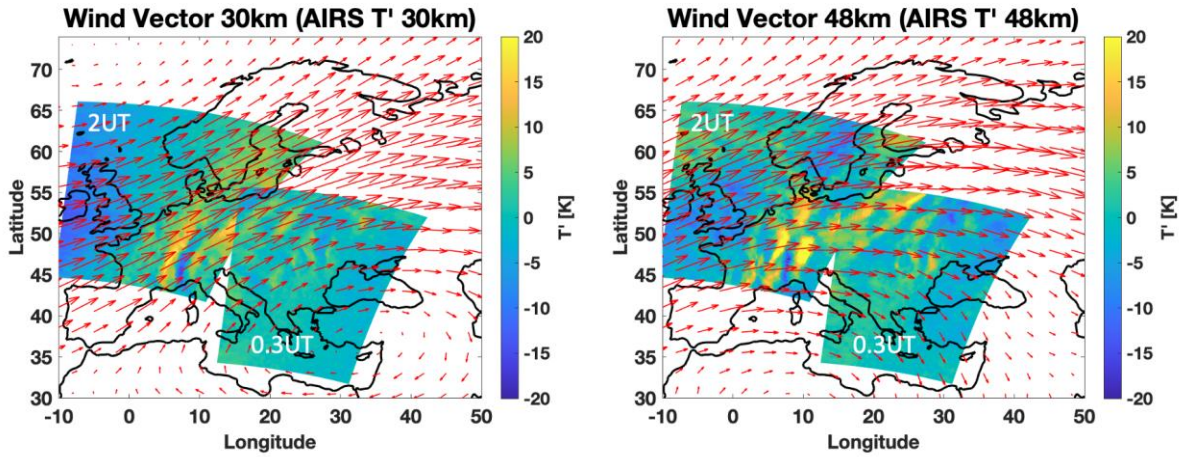

Figure 7: AIRS derived T' swaths at 2UT and 0.3UT with wind vectors at 30km (left) and 48km (right).

Vertical profiles of the AIRS measurements plotted with MERRA-2 winds and temperatures over the same region are given in Figure 8. While MERRA-2 does not have the resolution to detect all GWs present, and may also be presenting data from assimilated instruments, it is noted here that GWs with a similar characteristic to the observed MWs at 2UT are present in the MERRA-2 reanalysis data at much lower amplitudes (Figure 8a). These waves appear to be present from 6-30^{o}E with decreasing λ_z going further towards the East. This would be unsurprising for trailing MWs given the decreasing zonal winds in the stratosphere changing from 100ms^{-1} near 5^{o}E at z=45km to 50ms^{-1} near 25^{o}E shown in Figure 8b. This decrease in λ_z along with likely dissipation of trailing waves as they travel further from the source would contribute to a smaller *T'* observed by AIRS due to the vertical averaging associated with AIRS temperature retrievals. Evidence of shorter λ_z waves (~12km) is observed between 15-20^{o} longitude in the AIRS measurements (Figure 8d). These GWs are potentially trailing MWs. However, also apparent in these AIRS measurements are GW perturbations between 25-30^{o}E which are superimposed on top of the presumed trailing waves. Plotted topography just to the

south in Figure 8e demonstrates two distinct regions of mountains which would both independently generate MWs. The waves further to the east overlap the Carpathian Mountains. Given the distinct location of these waves over mountains, and the lack of significant T' observed in between these two mountainous regions, it is unlikely that these waves between 25-30^{o}E are trailing waves. Instead these are likely MWs generated directly from topography nearby.

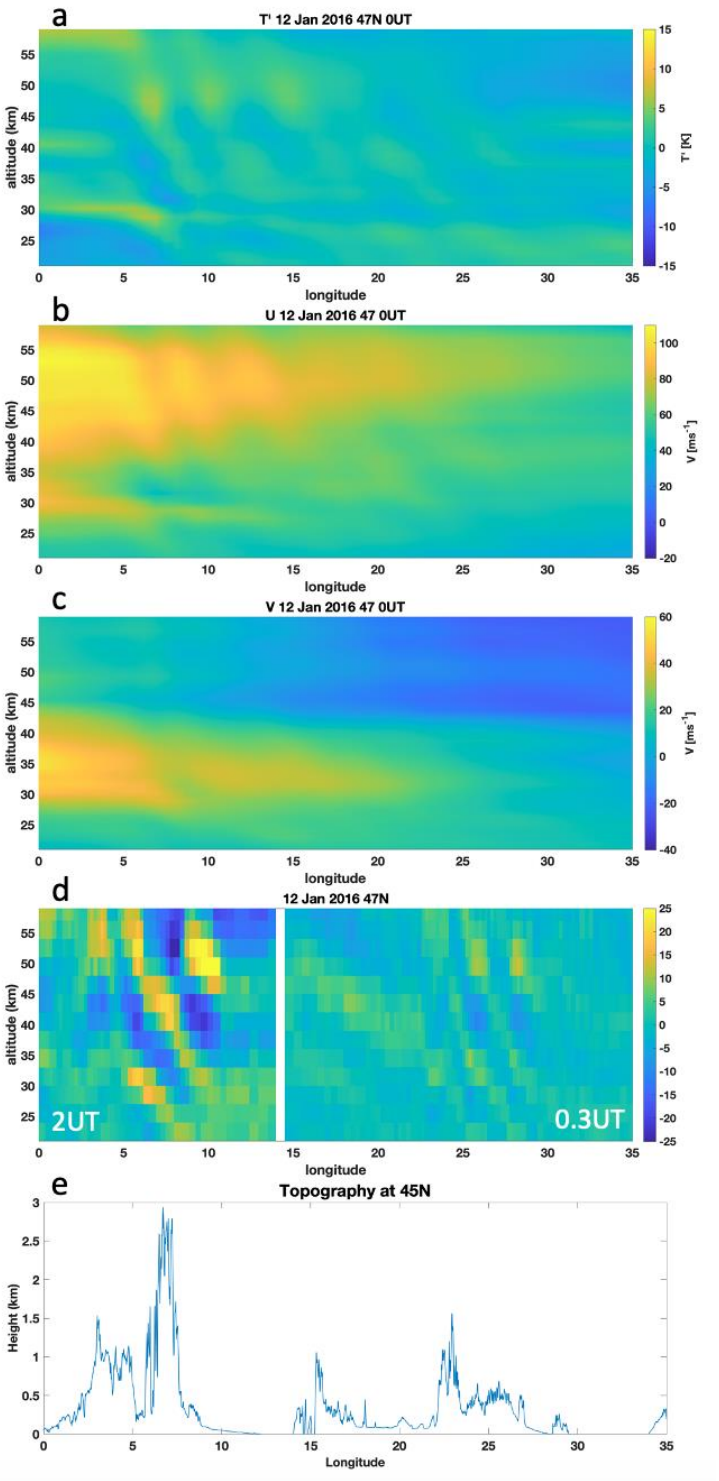

228

229 Figure 8: Plots of MERRA2 a) T', b) U, and c) V along the same longitude 47^{o} N as d) AIRS

230 derived T'. Plot e) shows topography at 45N where the highest mountain ridges are located near

231 AIRS MWs observations.

2.2 Event 2: Stratospheric Vortex Generated Waves

About nine hours after AIRS observed the large amplitude MW, the instrument sampled non-orographic PNJ-generated GWs extending from ~17°-27°E and 50°-57°N. At 11.6UT, AIRS *T'* indicated the presence of GWs with horizontal wavelengths of ~300km. Figures 9a-f show swaths of AIRS derived *T'* at six different altitudes. No discernable *T'* are visible near 42km in Figure 9d. However, *T'* associated with the observed GW are visible above and below this altitude with similar spatial orientation and horizontal wavelengths. Figure 9b shows traces of spatial paths used for vertical slices, which are shown in Figure 10. Figures 10a and 10b show west-to-east transects following the 52°N and 54°N latitude circles. Figure 10c shows a south-to-north transect along the 23°E meridian. All three perspectives demonstrate waves that disappear near 42km, with a changing orientation and propagation direction above and below 42km. This indicates the generation region of the observed GW may be near 42km. Figure 10c shows that the strongest *T'* appear between 50-55°N in latitude, with maximum *T'* ~5-7K. Figure 11a shows MERRA-2 vertical profiles of meridional and zonal winds at a latitude equatorward of the PNJ (48°N) and at a latitude within the PNJ core (54°N) averaged longitudinally from 8-33°E over the region of GWs observed in AIRS. Figures 11b and 11c show latitude-altitude sections of zonal and meridional winds. The strongest observed *T'* between 50-55°N also coincide with a region of strong meridional shear in the horizontal winds (both dV/dy and dU/dy). It is noted that there are multiple regions of shear, and consequently, several regions where wave generation may be possible. AIRS is most sensitive to larger vertical wavelengths, thus will observe those GWs with a larger vertical wavelength. A plot of MERRA-2 wind magnitudes and vectors at 42km and 12UT is shown in Figure 12. This wind view demonstrates the larger scale dynamics at play

causing disruptions to the PNJ through planetary wave disturbances in the region of the AIRS observed GWs.

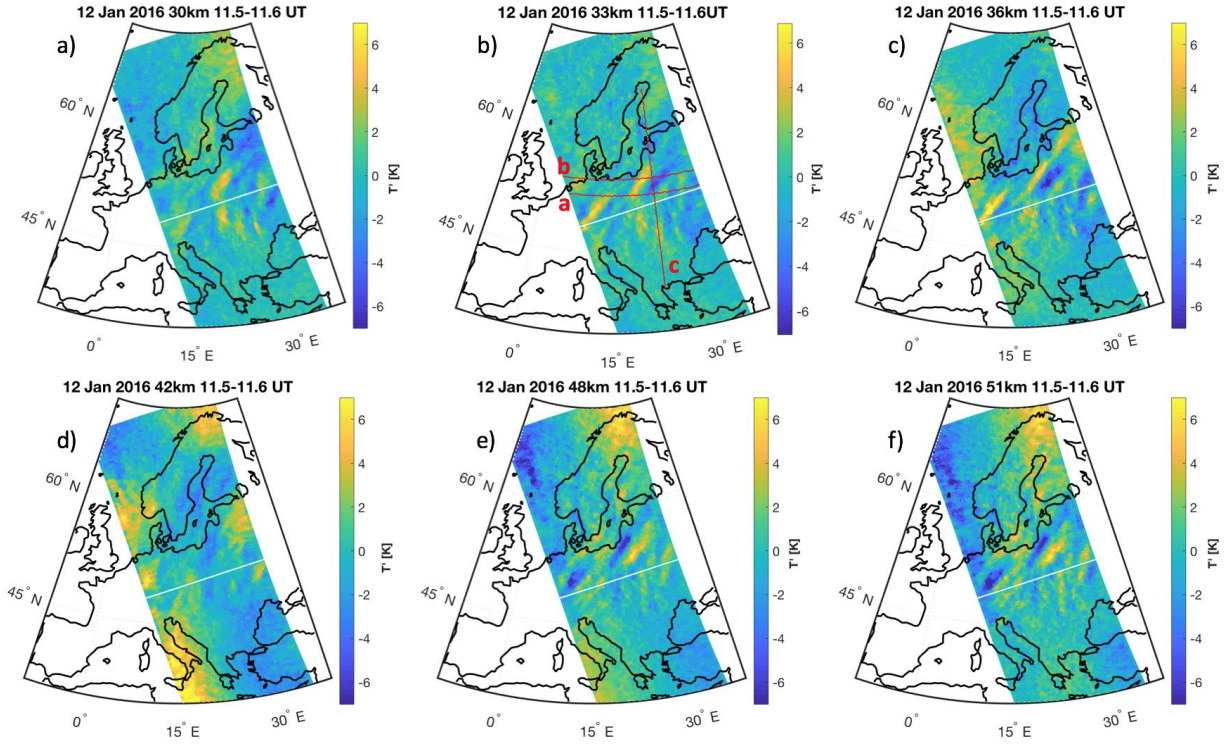

Figure 9: Swaths of AIRS derived *T'* over eastern Europe at altitudes ranging from 30-51km at approximately 11.5-11.6UT on 12 January 2016. Red lines marked 'a', 'b', and 'c' in panel b indicate the location of the longitude-altitude and latitude altitude transects shown in Figure 10.

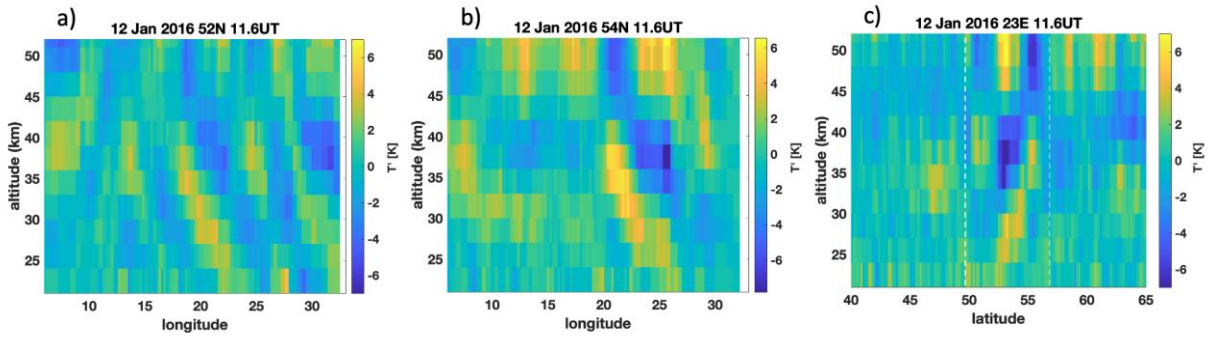

Figure 10: Panels ‘a’ and ‘b’ show longitude-altitude sections of AIRS *T’* at 52°N and 54°N respectively. Panel ‘c’ shows a latitude-altitude section along the 23°E longitude. The white dotted lines in panel ‘c’ denote a region of large dU/dy and dV/dy shown in Figure 11 b-c.

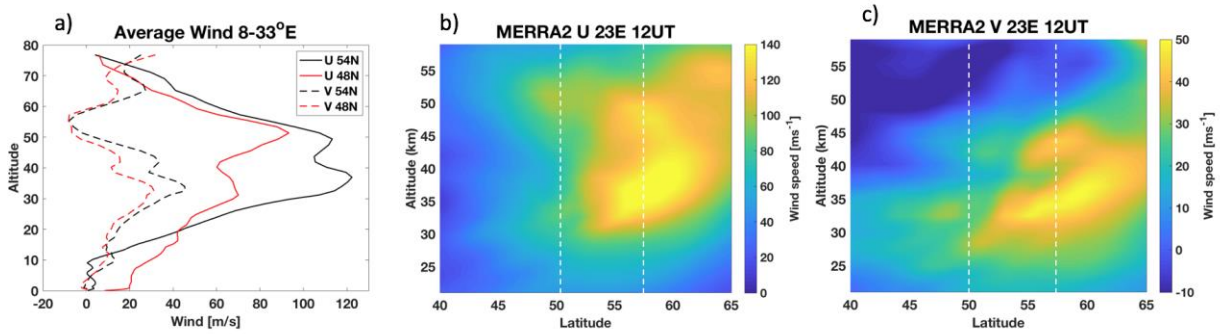

Figure 11: Panel ‘a’ shows zonal (solid lines) and meridional (dashed lines) wind profiles from MERRA-2 at 48°N (red) and 54°N (black) averaged longitudinally over 8-33°E. Panels ‘b’ and ‘c’ show latitude-altitude sections of zonal and meridional winds along the same path as Figure 10c. White dotted lines indicate the same region as those shown in Figure 10c.

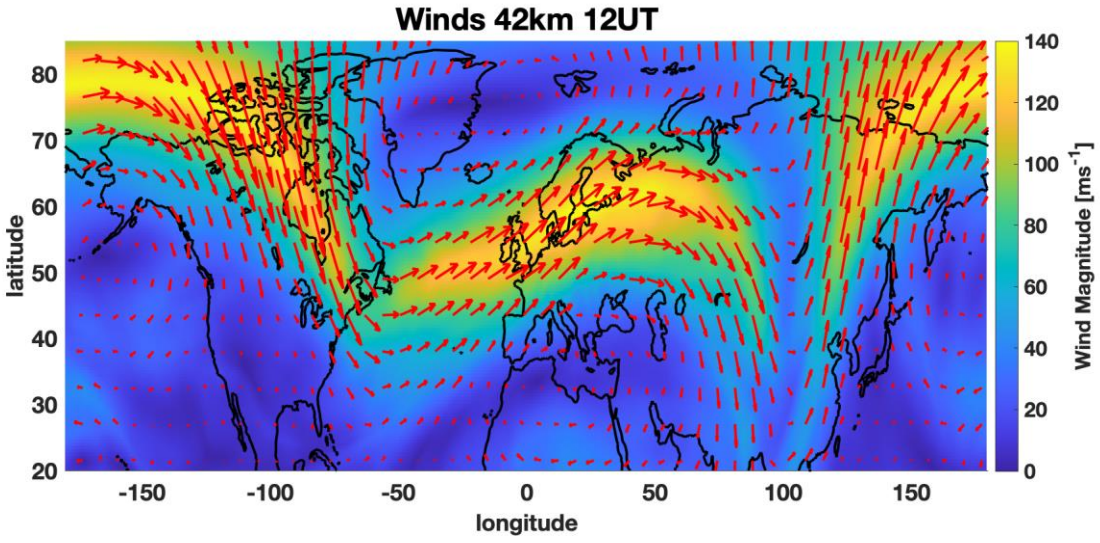

Figure 12: MERRA-2 wind magnitude and wind vectors at z=42 km and 12 UT.

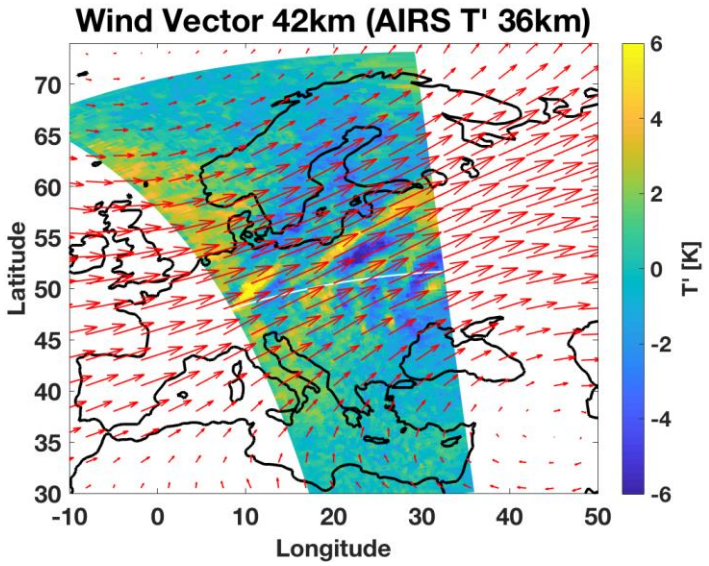

Figure 13: MERRA-2 wind vectors at 42km on 12 January 2016 at 12 UT plotted over AIRS *T'* at 36km at 11.5-11.6 UT.

The MERRA-2 wind vector at 42km and 12 UT plotted over AIRS *T'* at 36km and 11.5-11.6 UT is shown in Figure 13. The GWs generated near the peak of the PNJ have phase fronts aligned parallel with the wind vector in this region. This is consistent with the results of Sato and Yoshiki (2008) for GWs being generated by the PNJ due to spontaneous emission. The phase fronts of the GWs are also aligned southwest to northeast, which implies that they are propagating either southeastward or northwestward. Either wave could be generated from a southeastward or northwestward body force. This generation mechanism resulting from a body force has previously been discussed in Vadas et al., (2003, 2018). In the context of event 2, the body force assumed in that theory would correspond to a self-induced perturbation of quasi-geostrophic imbalance of the polar vortex, leading to the vortex-generated GWs. The amplitude of these observed GWs is about 1/5 of those MWs propagating to the stratosphere shown in event 1 despite similar λ_z between 30-40km, and hence similar AIRS vertical averaging. Such an amplitude difference is expected for localized stratospheric generation of GWs versus those GWs

which have grown over several scale heights, in analogy to the amplitude difference of secondary versus primary GWs [*Vadas et al*., 2003; *Vadas et al.*, 2018].

Finally, those GWs which are generated locally by the PNJ due to acceleration/deceleration from nonlinear dynamics of the PNJ would be expected to have upward and downward propagating components [*Sato et al*., 1999]. While downward versus upward propagation cannot be unequivocally determined from the AIRS data, it is proposed here that the observed GWs may be generated near the 42km level and may propagate upward above and downward below this level, similar to in situ generation from the PNJ discussed in Sato et al. (1999). This would result in upward and downward propagating GWs generated with the same propagation direction and horizontal wavelengths. The orientation of the GW phase lines in Figure 10 indicates that if the GWs are downward propagating below 42km then they are propagating towards the southeast, and above 42km if the GWs are propagating upward then they are also propagating towards the southeast. GWs generated from a body force near 42km have equal amplitudes for the same intrinsic horizontal phase speeds (in the frame of reference of the background winds) [Vadas et al., 2018]. From Figure 11, the wind is northeastward at 42km. Above this altitude, the wind is strongly eastward (increasing eastward as z increases), and below, the wind is more strongly northward (increasing northward as z decreases). Therefore, upward and downward southward propagating GWs would propagating into very different wind environments.

3. Discussion and Conclusions

AIRS measurements on 12 January 2016 showed significant *T'* associated with GWs over Europe. The sources of these observed GWs contributing to the *T'* were investigated over the region of western Europe and Scandinavia. Different sources of GWs were found to contribute to

313 *T'* variances during this period. The strongest of these stratospheric GWs were MWs arising due
314 to flow over the Alps. MWs are especially sensitive to stratospheric winds associated with the
315 PNJ in addition to tropospheric wind forcing over the mountainous region. In the case of MWs
316 observed on this day, peak amplitudes near 50km in altitude reached ~25-30K when the PNJ
317 winds were strong and persistent 30-60km. Weaker MWs were also observed ~1000 km to the
318 East over the Carpathian Mountains. These MWs encountered weaker winds in the stratosphere
319 and had lower amplitudes. It is also likely that trailing waves are present between this region.
320 However, the largest amplitude GWs detected in AIRS originate from sources near or below the
321 observation. MWs were not clearly observed at later times near 13UT, and we show that this is
322 due to a change in surface forcing conditions over the mountains.
323 Another source of GWs observed by AIRS on this day is the PNJ itself. GWs generated
324 in the stratosphere have lower amplitudes, ~1/5 the amplitude of those MWs generated in the
325 troposphere, which grow in amplitude as they propagate up to stratosphere. Additionally, AIRS
326 vertical temperature measurements provide a unique look at the GW phase changes that occur as
327 a function of altitude for GWs generated near the peak of the PNJ. GWs generated near the PNJ
328 appear to have upward and downward propagation directions similar to secondary GWs
329 generated in this region (e.g., as shown in observations presented by Vadas et al., 2018). In the
330 case observed by AIRS, vertical wavelengths were long enough to be within the threshold of
331 detection of AIRS. However, it should be noted that smaller vertical wavelengths that would not
332 be observed by AIRS may also be generated by the PNJ [*Yoshiki and Sato,* 2000]. It is also
333 emphasized here that there are several regions of increased shear at multiple altitudes within the
334 PNJ during this time period. These also have the potential to generate GWs at different scales
335 and over different regions. Such jet-generated GWs may be present as well, and may cause

constructive and destructive interference among existing waves. Unfortunately, AIRS does not have the vertical resolution to detect all of these smaller vertical scales that may also be present.

In the case study shown here, the PNJ plays a significant role in the propagation and generation of the GWs observed by AIRS. Orographic GWs generated in the troposphere with a favorable propagation orientation experience amplitude growth in the region of the PNJ due to the absence of instability and breaking in regions of increasing winds. The PNJ also has the potential to generate GWs similar to tropospheric jet-generated GWs. AIRS observed significant GW activity on this day over the region of overlap between the Alps, the tropospheric jet, and the PNJ. These observations demonstrate that there can be multiple sources of GWs active in the same region, all of which play a role in momentum transport in the stratosphere and at altitudes above this region.

Acknowledgments

Research by Dr. Bossert was supported under NSF grant AGS-1822585, and Dr. Vadas was supported under NSF grant AGS-822867. VLH acknowledges support under NASA grant 80NSSC19K0834. We acknowledge Dr. Andreas Dörnbrack for thoughtful discussion and feedback. AIRS data are publicly available at https://airs.jpl.nasa.gov/data/get_data. The AIRS gravity wave data sets used in this study can be obtained from https://datapub.fz-juelich.de/slcs/airs/gravity_waves/index.html. MERRA-2 data are available at MDISC, managed by the NASA Goddard Earth Sciences (GES) Data and Information Services Center (DISC) at https://disc.sci.gsfc.nasa.gov/datasets/M2I6NVANA_5.12.4/keywords=MERRA-2 and https://disc.gsfc.nasa.gov/SSW/#keywords=MERRA-2.

References

Alexander, M. J. and C. Barnett (2007), Using Satellite Observations to Constrain Parameterizations of Gravity Wave Effects for Global Models, J. Atmos. Sci., 64, 1652-1665, doi: 10.1175/JAS387.1

Alexander, M. J., and H. Teitelbaum (2007), Observation and analysis of a large amplitude mountain wave event over the Antarctic peninsula, *J. Geophys. Res*. 112, D21103, doi:10.1029/2006JD008368.

Alexander, M. J., Geller, M. , McLandress, C. , Polavarapu, S. , Preusse, P. , Sassi, F. , Sato, K. , Eckermann, S. , Ern, M. , Hertzog, A. , Kawatani, Y. , Pulido, M. , Shaw, T. A., Sigmond, M., Vincent, R. and Watanabe, S. (2010), Recent developments in gravity-wave effects in climate models and the global distribution of gravity-wave momentum flux from observations and models. Q.J.R. Meteorol. Soc., 136: 1103-1124. doi:10.1002/qj.637

Amante, C. And B. W. Eakins (2009), ETOPO1 1 Arc-Minute Global Relieve Model: Procedures, Data Sources and Analysis. NOAA Technical Memorandum NESDIS NGDC-24. National Geophysical Data Center, NOAA, doi:10.7289/V5C8276M.

Becker, E. and S. L. Vadas (2018), Secondary gravity waves in the winter mesosphere: Results from high-resolutions, gravity-wave resolving global circulation model, *J. Geophys. Res. Atmos.*, 123, doi:10.1002/2017JD027460.

Bosilovich, M., S. Akella, L. Coy, R. Cullather, C. Draper, R. Gelaro, et al. (2015). MERRA-2: Initial evaluation of the climate, NASA Tech. Rep. Series on Global Modeling and Data Assimilation, NASA/TM–2015-104606 (Vol. 43, 139 pp.).

Bossert, K., D. C. Fritts, P.-D. Pautet, B. P. Williams, M. J. Taylor, B. Kaifler, A. Dörnbrack, I. M. Reid, D. J. Murphy, A. J. Spargo, and A. D. MacKinnin (2015), Momentum flux estimates accompanying multiscale gravity waves over Mount Cook, New Zealand, on 13 July 2014 during the DEEPWAVE campaign, *J. Geophys. Res*., DOI: 10.1002/2015JD023197.

Bossert, K., C. G. Kruse, C. J. Heale, D. C. Fritts, B. P. Williams, J. B. Snively, P.-D. Pautet, and M. J. Taylor (2017), Secondary gravity wave generation over New Zealand during the DEEPWAVE campaign, *J. Geophys. Res. Atmos. 122*, doi:10.1002/2016JD026079.

Bramberger, M., Dörnbrack, A., Bossert, K., Ehard, B., Kaifler, B.,Mallaun, C., Orr, A., Pautet, P.-D., Rapp, M., Taylor, M. J., Vosper, S., Williams, B. P., andWitschas, B. (2017), Does Strong tropospheric forcing cause large-amplitude mesospheric gravity waves? A DEEPWAVE case study. Journal of Geophysical Research: Atmospheres, 122, 11,422–11,443, https://doi.org/10.1002/2017JD027371.

Bramberger, M., A. Dornbrack, H. Wilms, S. Gemsa, K. Raynor, and R. Sharman (2018), Vertically Propagating Mountain Waves – A Hazard for High-Flying Aircraft?, J. Appl. Meteor. Climatol., 57, 1957-1975, doi:10.1175/JAMC-D-17-0340.1.

Bramberger, M., A. Dornbrack, H. Wilms, F. Ewald, and R. Sharman (2020), Mountain Wave Turbulence Encounter of the Research Aircraft HALO above Iceland, J. Appl. Meteor. Climatol., 0 doi:10.1175/JAMC-D-19-0079.1.

401 Buss, S., A. Hertzog, C. Hostettler, T. P. Bui, D. Luthi, and H. Wernli (2004), Analysis of a jet
402 stream induced gravity wave associated with an observed stratospheric ice cloud over
403 Greenland, Atmos. Chem. Phys., 4, 1183-1200.
404 Chu, X., Zhao, J., Lu, X., Harvey, V. L., Jones, R. M., Becker, E., C. Chen, W. Fong, Z. Yu,
405 B. R. Roberts, A. Dornbrack (2018), Lidar observations of stratospheric gravity waves from
406 2011 to 2015 at McMurdo (77.84°S, 166.69°E), Antarctica: 2. Potential energy densities,
407 lognormal distributions, and seasonal variations. *Journal of Geophysical Research:*
408 *Atmospheres*, 123, 7910– 7934. https://doi.org/10.1029/2017JD027386
409 Dörnbrack, A., Gisinger, S., Kaifler, N., Portele, T. C., Bramberger, M., Rapp, M., Gerding, M.,
410 Söder, J., Žagar, N., and Jelić, D. (2018), Gravity waves excited during a minor sudden
411 stratospheric warming, Atmos. Chem. Phys., 18, 12915-12931, https://doi.org/10.5194/acp-
412 18-12915-2018.
413 Dörnbrack, A., T. Birner, A. Fix, H. Flentje, A. Meister, H. Schmid, E. V. Browell, and M. J.
414 Mahoney (2002), Evidence for inertia gravity waves forming polar stratospheric clouds over
415 Scandinavia, J. Geophys. Res., 107(D20), 8287, doi:10.1029/2001JD000452.
416 Dörnbrack, A., M. Leutbecher, R. Kivi, and E. Kyro (1999), Mountain-wave-induced record low
417 stratospheric temperatures above northern Scandinavia, *Tellus A: Dynamic Meteorology and*
418 *Oceanography*, 51:5, 951-963, doi:10.3402/tellusa.v51i5.14504.
419 Ern, M., L. Hoffmann, and P. Preusse (2017), Directional gravity wave momentum fluxes in the
420 stratosphere derived from high-resolution AIRS temperature data, *Geophys. Res. Lett*., 44,
421 475-485, doi:10.1002/2016GL072007.
422 Ehard, B., B. Kaifler, A. Dornbrack, P. Preusse, S. D. Eckermann, M. Bramberger, S. Gisinger,
423 N. Kaifler, B. Liley, J. Wagner, and M. Rapp (2017b), Horizontal propagation of large-

amplitude mountain waves into the polar night jet, J. Geophys. Res. Atmos., 122, 1423–1436, doi:10.1002/2016JD025621.

Eckermann, S. D., J. D. Doyle, P. A. Reinecke, C. A. Reynolds, R. B. Smith, D. C. Fritts, and A. Dornbrack (2019), Stratospheric Gravity Wave Products from Satellite Infrared Nadir Radiances in the Planning, Execution, and Validation of Aircraft Measurements during DEEPWAVE, *J. Appl. Meteor. Climatol.*, 58, 2049-2075, doi:10.1175/JAMC-D-19-0015.1.

Eckermann, S.D., D. Broutman, J. Ma, J.D. Doyle, P. Pautet, M.J. Taylor, K. Bossert, B.P. Williams, D.C. Fritts, and R.B. Smith, (2016), Dynamics of Orographic Gravity Waves Observed in the Mesosphere over the Auckland Islands during the Deep Propagating Gravity Wave Experiment (DEEPWAVE). *J. Atmos. Sci.,* **73**, 3855–3876, https://doi.org/10.1175/JAS-D-16-0059.1

Ern, M., Trinh, Q. T., Preusse, P., Gille, J. C., Mlynczak, M. G., Russell III, J. M., and Riese, M.: GRACILE: a comprehensive climatology of atmospheric gravity wave parameters based on satellite limb soundings, Earth Syst. Sci. Data, 10, 857–892, https://doi.org/10.5194/essd-10-857-2018, 2018.

Fritts, D. C., and Z. Luo (1992), Gravity Wave Excitation by Geostrophic Adjustment of the Jet Stream. Part I: Two-Dimensional Forcing, *J. of Atmos. Sci. 49(8)*, 681-697, doi:10.1175/1520-0469.

Fritts, D. C., and M. J. Alexander (2003), Gravity wave dynamics and effects in the middle atmosphere, *Rev. Geophys., 41*(1), 1003, doi:10.1029/2001RG000106.

Fritts, D.C., R.B. Smith, M.J. Taylor, J.D. Doyle, S.D. Eckermann, A. Dörnbrack, M. Rapp, B.P. Williams, P. Pautet, K. Bossert, N.R. Criddle, C.A. Reynolds, P.A. Reinecke, M. Uddstrom, M.J. Revell, R. Turner, B. Kaifler, J.S. Wagner, T. Mixa, C.G. Kruse, A.D. Nugent, C.D.

Watson, S. Gisinger, S.M. Smith, R.S. Lieberman, B. Laughman, J.J. Moore, W.O. Brown, J.A. Haggerty, A. Rockwell, G.J. Stossmeister, S.F. Williams, G. Hernandez, D.J. Murphy, A.R. Klekociuk, I.M. Reid, and J. Ma, (2016), The Deep Propagating Gravity Wave Experiment (DEEPWAVE): An Airborne and Ground-Based Exploration of Gravity Wave Propagation and Effects from Their Sources throughout the Lower and Middle Atmosphere. *Bull. Amer. Meteor. Soc.,* **97**, 425–453, doi.org/10.1175/BAMS-D-14-00269.1

Garcia, R. R. and S. Solomon (1985), The Effect of Breaking Gravity Waves on the Dynamics and Chemical Composition of the Mesosphere and Lower Thermosphere, *J. Geophys. Res.* 90, D2, 3850-3868.

Giez, A., C. Mallaun, M. Zoger, A. Dornbrack, and U. Schumann (2016), Comparison of static pressure from aircraft trailing cone measurements and numerical weather prediction analysis. AIAA, Atmospheric Flight Mechanics Conf., Washington, DC, AIAA, doi:10.2514/6.2016-3707.

Gisinger, S., A. Dörnbrack, V. Matthias, J.D. Doyle, S.D. Eckermann, B. Ehard, L. Hoffmann, B. Kaifler, C.G. Kruse, and M. Rapp, 2017: Atmospheric Conditions during the Deep Propagating Gravity Wave Experiment (DEEPWAVE). *Mon. Wea. Rev.*, **145**, 4249–4275, https://doi.org/10.1175/MWR-D-16-0435.1

Gong, J., D.L. Wu, and S.D. Eckermann (2012), Gravity wave variances and propagation derived from AIRS radiances, Atmos. Chem. Phys., 12, 1701–1720, doi:10.5194/acp-12- 1701-2012.

Harvey, V. L., R. B. Pierce, T. D. Fairlie, and M. H. Hitchman (2002), A climatology of stratospheric polar vortices and anticyclones, *J. Geophys. Res., 107*(D20), 4442, doi:10.1029/2001JD001471.

Heale, C., K. Bossert, S. L. Vadas, L. Hoffmann, A. Dörnbrack, G. Stober, J. B. Snively, C. Jacobi (2020), Secondary Gravity Waves Generated by Breaking Mountain Waves over Europe, *J. Geophys. Res. Atmos*., doi:10.1029/2019JD031662

Heale, C., K. Bossert, J. Snively, D. C. Fritts, P.-D. Pautet, and M. J. Taylor (2017), Numerical modeling of a multiscale gravity wave event and its airglow signatures over Mount Cook, New Zealand during the DEEPWAVE campaign, *J. Geophys. Res.,* doi:10.1002/2016JD025700.

Hoffmann, L., M. J. Alexander, C. Clerbaux, A. W. Grimsdell, C. I. Meyer, T. Rossler, and B. Tournier (2014), Intercomparison of stratospheric gravity wave observations with AIRS and IASI, *Atmos. Meas. Tech., 7*, 4517-4537, doi:10.5194/amt-7-4517-2014.

Hoffmann, L., X. Xue, and M. J. Alexander (2013), A global view of stratospheric gravity wave hotspots located with Atmospheric Infrared Sounder observations, *J. Geophys. Res. Atmos. 118*, 416-434, doi:10.1029/2012JD18658.

Hoffmann, L., and M. J. Alexander (2009), Retrieval of Stratospheric Temperatures from AIRS Radiance Measurements for Gravity Wave Studies, *J. Geophys. Res*., 114, D07105, doi:10.1029/2008JD011241.

Hoffmann, L. H., A. W. Grimsdell, and M. J. Alexander (2016), Stratospheric gravity waves at Southern Hemisphere orographic hotspots: 2003-2014 AIRS/Aqua observations, *Atmos. Chem. Phys., 16,* 938109397, doi:10.519/acp-16-9381.

Holton, J. R. (1983), The Influence of Gravity Wave Breaking on the General Circulation of the Middle Atmosphere, *J. Atmos. Sci.*, 40, 2497-2507.

Holton, J. R. (1982), The role of gravity wave induced grad and diffusion in the momentum budget of the mesosphere, *J. Atmos. Sci*., 39, 791–799.

492 Jiang, Q., J. D. Doyle, S. D. Eckermann, and B. P. Williams (2019), Stratospheric Trailing
493 Gravity Waves from New Zealand, J. Atmos. Sci, 76, 1565-1587, doi:10.1175/JAS-D-18-
494 0290.1.
495 Jiang, J. H., D. L. Wu, S. D. Eckermann, and J. Ma (2003), Mountain waves in the middle
496 atmosphere: Microwave limb sounder observations and analyses, Advances Space Res., 32,
497 801-806. DOI:10.106/S0273-1177(03)00402-2.
498 Jiang, Q., J. D. Doyle, A. Reinecke, R. B. Smith, S. D. Eckermann (2012), A modeling study of
499 stratospheric waves over the southern Andes and drake passage, *J. of Atmos. Sci.*,
500 DOI:10.1175/JAS-D-12-0180.1.
501 Jiang, J. H., S. D. Eckermann, D. L. Wu, K. Hocke, B. Wang, J. Ma, Y. Zhang (2005), Seasonal
502 variation of gravity wave sources from satellite observation, Advances in Space Res., 35,
503 1925-1932.
504 Krisch, I., P. Preusse, J. Ungermann, A. Dornbrack, S. D. Eckermann, M. Ern, F. Friedel-Vallon,
505 M. Kaufmann, H. Oelhaf, M. Rapp, C. Strube, and M. Riese (2017), First tomographic
506 observations of gravity waves by the infrared limb imager GLORIA, *Atmos. Chem. Phys.*, **17**,
507 14937-14953, doi:10.5194/acp-17-14937-2017.
508 Kruse, C.G., R.B. Smith, and S.D. Eckermann, 2016: The Midlatitude Lower-Stratospheric
509 Mountain Wave "Valve Layer". *J. Atmos. Sci.*, **73**, 5081–5100,https://doi.org/10.1175/JAS-D-
510 16-0173.1
511 Liu, X., Xu, J., Yue, J., Vadas, S. L., & Becker, E. (2019), Orographic primary and secondary
512 gravity waves in the middle atmosphere from 16-year SABER observations. *Geophysical*
513 *Research Letters*, 46. https://doi.org/10.1029/2019GL082256.
514 Llamedo, P., J. Salvador, A. de la Torre, J. Quiroga, P. Alexander, R. Hierro, T. Schmidt, A.

Pazmino, and E. Quel (2019), 11 Years of Rayleigh Lidar Observations of Gravity Wave Activity Above the Southern Tip of South America, *Journal of Geophysical Research: Atmospheres, 124*, 451-467. doi:10.1029/2018JD028673.

Mallaun, C., A. Giez, and R. Baumann (2015), Calibration of 3-D wind measurements on a single-engine research aircraft, Atmos. Meas. Tech., 8, 3177-3196, doi:10.5194/amt-8-3177-2015.

Meyer, C. I., and L. Hoffmann (2014), Validation of AIRS high-resolution stratospheric temperature retrievals, *Proc. SPIE 9242, Remote Sensing of Clouds and the Atmosphere XIX; and Optics in Atmospheric Propagation and Adaptive Systems XVII, 92420L*, doi:10.1117/12.2066967.

Molod, A., Takacs, L., Suarez, M., & Bacmeister, J. (2015). Development of the GEOS-5 atmospheric general circulation model: Evolution from MERRA to MERRA2. Geoscientific Model Development, 8, 1339–1356. https://doi.org/10.5194/gmd-8-1339-2015

O'Sullivan, D. and T. J. Dunkerton (1995), Generation of Inertia–Gravity Waves in a Simulated Life Cycle of Baroclinic Instability. J. Atmos. Sci., 52, 3695–3716, https://doi.org/10.1175/1520-0469(1995)052<3695:GOIWIA>2.0.CO;2

Plougonven, R., C. Snyder (2007), Inertia-Gravity Waves Spontaneously Generated by Jets and Fronts. Part I: Different Baroclinic Life Cycles, *J. Atmos. Sci, 64*, doi:10.1175/JAS3953.1.

Plougonven, R., and F. Zhang (2014), Internal gravity waves from atmospheric jets and fronts, Rev. Geophys., 52(1), 33-76, doi:10.1002/2012RG000419

Preusse, P., S. D. Eckermann, M. Ern, J. Oberheide, R. H. Picard, R. G. Roble, M. Riese, J. M. Russell III, and M. G. Mlynczak (2009), Global ray tracing simulations of the SABER gravity wave climatology, *J. Geophys. Res*. 114, D08126, doi:10.1029/2008JD011214.

538 Randall, C. E., Carstens, J., France, J. A., Harvey, V. L., Hoffmann, L., Bailey, S. M., Alexander,
539 M. J., Lumpe, J. D., Yue, J., Thurairajah, B., Siskind, D. E., Zhao, Y., Taylor, M. J., &
540 Russell, J. M. III (2017). New AIM/CIPS global observations of gravity waves near 50-55
541 km. Geophysical Research Letters, 44, 7044– 7052. https://doi.org/10.1002/2017GL073943.
542 Sato, K., T. Kumakura, and M. Takahashi (1999), Gravity Waves Appearing in a High-Resolution
543 GCM Simulation, *J. Atmos. Sci.*, ***56***, *8*,1005-1018.
544 Sato, K. (2000), Sources of gravity waves in the middle atmosphere, *Adv Polar Upper Atmos Res*
545 **14**, 233–240.
546 Sato, K. and M. Yoshiki (2008), Gravity Wave Generation around the Polar Vortex in the
547 Stratosphere Revealed by 3-Hourly Radiosonde Observations at Syowa Station, *J. Atmos. Sci*.,
548 ***65***, 3719-3735, doi:10.1175/2008JAS2539.1.
549 Senf, F., and U. Achatz (2011), On the impact of middle-atmosphere thermal tides on the
550 propagation and dissipation of gravity waves, *J. Geophys. Res*., 116, D24110,
551 doi:10.1029/2011JD015794.
552 Schmidt, T., P. Alexander, and A. de la Torre (2016), Stratospheric gravity wave momentum flux
553 from radio occultations, *J. Geophys. Res. Atmospheres*, doi:10.1002/2015JD024135.
554 Tsuda, T., M. Nishida, C. Rocken, and R. H. Ware (2000), A Global Morphology of Gravity
555 Wave Activity in the Stratosphere Revealed by the GPS Occultation Data (GPS/MET), *J.*
556 *Gophys. Res.*, 105, D6, 7257-7273.
557 Smith, R. B., B. K. Woods, J. Jensen, W. A. Cooper, J. D. Doyle, and Q. Jiang, and V. Grubisic
558 (2008), Mountain Waves entering the stratosphere, *J. Atmos. Sci*., 65, 2543-2562,
559 doi:10.1175/2007JAS2598.1.
560 Smith, R. B., A. D. Nugent, C. G. Kruse, D. C. Fritts, J. D. Doyle, S. D. Eckermann, M. J. Taylor,

561 A. Dornbrack, M. Uddstrom, W. Cooper, P. Romashkin, J. Jensen, S. Beaton (2016),
562 Stratospheric Gravity Wave Fluxes and Scales during DEEPWAVE, *J. Atmos. Sci*., 73,
563 doi:10.1175/JAS-D-15-0324.1.
564 Uccellini, L. W., and S. E. Koch (1987), The synoptic setting and possible energy sources for
565 mesoscale wave disturbances. Mon. Wea. Rev., 115, 721–729, https://doi.org/10.1175/1520-
566 0493(1987)115<0721:TSSAPE>2.0.CO;2.
567 Vadas, S. L., D. C. Fritts, and M. J. Alexander (2003), Mechanism for the Generation of Secondary
568 Waves in Wave Breaking Regions, *J. Atmos. Sci.*, 60, 194-214.
569 Vadas, S. L., Zhao, J., Chu, X., and Becker, E. (2018), The excitation of secondary gravity waves
570 from local body forces: Theory and observation. *Journal of Geophysical Research:*
571 *Atmospheres*, *123*, 9296–9325. https://doi.org/10.1029/2017JD027970.
572 Vadas, S. L., and E. Becker (2019), Numerical modeling of the generation of tertiary gravity
573 waves in the mesosphere and thermosphere during strong mountain wave 804 events over the
574 Southern Andes, J. Geophys. Res. Space Physics, 124, doi:10.1029/2019JA026694.
575 Wagner, J., A. Dornbrack, M. Rapp, S. Gisinger, B. Ehard, M. Bramberger, B. Witschas, F.
576 Chouza, S. Rahm, C. Maullun, G. Baumgarten, and P. Hoor (2017), Observed versus
577 simulated mountain waves over Scandinavia-improvement of vertical winds, energy and
578 momentum fluxes by enhanced model resolution?, Atmos. Chem. Phys., **17**, 4031-4052,
579 doi:10.5194/acp-17-4031-2017.
580 Wang, S., F. Zhang, and C. Snyder (2008), Generation and Propagation of Inertia-Gravity Waves
581 from Vortex Dipoles and Jets, *J. Atmos. Sci*., **66**, 1294-1314, doi:10.1175/2008JAS2830.1.
582 Witschas, B., S. Rahm, A. Dornbrack, J. Wagner, and M. Rapp, (2017), Airborn Wind Lidar
583 Measurements of Vertical and Horizontal Winds for the Investigation of Orographically
584 Induced Gravity Waves, *J. Atmos. Oceanic Technol*., **34**, 1371-1386, doi:10.1175/JTECH-D-

17-0021.1

Woods, B. K., and R. B. Smith (2010), Energy Flux and Wavelet Diagnostics of Secondary Mountain Waves, *J. Atmos. Sci*., **67**, 3721-3738, doi:10.1175/2009JAS3285.1.

Wright, C. J., N. P. Hindley, L. Hoffmann, M. J. Alexander, and N. J. Mitchell (2017), Exploring gravity wave characteristics in 3-D using a novel S-transform technique: AIRS/Aqua measurements over the Southern Andes and Drake Passage, *Atmos. Chem. Phys.*, **17**, DOI:10.5194/acp-17-8553-2017.

Wu, D.L. and S.D. Eckermann, 2008: Global Gravity Wave Variances from Aura MLS: Characteristics and Interpretation. *J. Atmos. Sci.*, **65**, 3695–3718,https://doi.org/10.1175/2008JAS2489.1

Wu, D. L., and F. Zhang (2004), A study of mesoscale gravity waves over the North Atlantic with Satellite observations and a mesoscale model, *J. Geophys. Res.*, *109*, D22104, doi:10.1029/2004JD005090.

Yamashita, C., Liu, H.-L., & Chu, X. (2010). Gravity wave variations during the 2009 stratospheric sudden warming as revealed by ECMWF-T799 and observations. Geophysical Research Letters, 37, L22806. https://doi.org/10.1029/2010GL045437.

Yamashita, C., England, S. L., Immel, T. J., & Chang, L. C. (2013). Gravity wave variations during elevated stratopause events using SABER observations. Journal of Geophysical Research – Atmospheres, 118, 5287– 5303. https://doi.org/10.1002/jgrd.50474.

Yoshiki, M., and K. Sato (2000), A statistical study of gravity waves in the polar regions based on operational radiosonde data, J. Geophys. Res., 105, doi:10.1029/2000JD900204.

Zhang, F. (2004), Generation of Mesoscale Gravity Waves in Upper-Tropospheric Jet-Front Systems, *J. Atmos. Sci.*, **61**, 440-457.

608

609

610